Quantitative brain imaging analysis of neurological syndromes associated with anti-GAD antibodies

Maëlle Dade [a,b], Marine Giry [b], Giulia Berzero [a], Marion Benazra [b], Gilles Huberfeld [c], Delphine Leclercq [d], Vincent Navarro [b,c], Jean-Yves Delattre [a,b], Dimitri Psimaras [a,b], Agusti Alentorn [a,b,*]

[a] AP-HP, Groupe Hospitalier Pitié-Salpêtrière, Neurology 2 Department Mazarin, F-75013 Paris, France
[b] Sorbonne Université, Inserm, CNRS, Paris Brain Institute, Institut du Cerveau et de la Moelle épinière, ICM, F-75013 Paris, France
[c] AP-HP, Groupe Hospitalier Pitié-Salpêtrière, Neurology Department, F-75013 Paris, France
[d] AP-HP, Groupe Hospitalier Pitié-Salpêtrière, Neuroradiology Department, F-75013 Paris, France

ARTICLE INFO

ABSTRACT

Neurological disorders associated with anti-glutamic acid decarboxylase (GAD) autoimmunity are rare and include a variety of neurological syndromes: stiff-person syndrome, cerebellar ataxia or limbic encephalitis. The diagnosis remains challenging due to the variety of symptoms and normal brain imaging.

The morphological MRI of 26 patients (T1-weighted and Fluid-attenuated inversion recovery (FLAIR)-weighted images) was analyzed at the initial stage of diagnosis, matched by age and sex to 26 healthy subjects. We performed a vertex-wise analysis using a generalized linear model, adjusting by age, to compare the brain cortical thickness of both populations. In addition, we used a voxel-based morphometry of cerebellum thickness obtained by CEREbellum Segmentation (CERES), as well as the hippocampus volumetry comparison using HIPpocampus subfield Segmentation (HIPS). Finally, we extracted 62 radiomics features using LifeX to assess the classification performance using a random forest model to identify an anti-GAD related MRI.

The results suggest a peculiar profile of atrophy in patients with anti-GAD, with a significant atrophy in the temporal and frontal lobes (adjusted p-value < 0.05), and a focal cerebellar atrophy of the V-lobule, independently of the anti-GAD phenotype. Finally, the MRIs from anti-GAD patients were correctly classified when compared to the control group, with an area under the curve (AUC) of 0.98.

This study suggests a particular pattern of cortical atrophy throughout all anti-GAD phenotypes. These results reinforce the notion that the different neurological anti-GAD phenotypes should be considered as a continuum due to their similar cortical thickness profiles.

1. Introduction

The field of autoimmune pathologies in the central nervous system has particularly developed in the last decades with the discovery of several antineuronal antibodies (Ab), associated with specific neurological phenotypes (Graus et al., 2010).

Glutamic acid decarboxylase (GAD) is an intracellular enzyme whose physiological role is the decarboxylation of glutamate into gamma-aminobutyric acid (GABA), mostly expressed in neuronal cells and in insulin-secreting β pancreatic cells (Vincent et al., 1983; Solimena and De Camilli, 1991).

Anti-GAD autoimmunity, leading to the destruction of these β cells of the pancreas, is known to be one of the causes of type 1 diabetes (Paschou et al., 2018). Disorders of the central nervous system is much rarer. They can be related to the alteration of the GABAergic transmission but their exact pathophysiology remains still not well elucidated (Tian et al., 1999; Jin et al., 2003; Koerner et al., 2004; Hansen et al., 2013). Anti-GAD autoimmunity is responsible for various neurological presentations, such stiff person syndrome (SPS), cerebellar ataxia (CAt), limbic encephalitis (LE) or temporal lobe epilepsy (TLE) (Saiz et al., 2008; McKeon and Tracy, 2017), and is rarely associated with cancers (Graus et al., 2020).

Conventional imaging contribution to the diagnosis is often limited (Meinck and Thompson, 2002). In the acute phase, Fluid-attenuated

inversion recovery (FLAIR)-weighted hyperintensities of hippocampal structures can be present in some cases of limbic encephalitis (Malter et al., 2010); at long term, hippocampal atrophy, cerebellar or more global atrophy have been described (Hadjivassiliou et al., 2017; Fredriksen et al., 2018; Ernst et al., 2019; Mitoma et al., 2018). Rare studies with volumetric analysis of limbic structures have been performed but only in a population of autoimmunity against GAD with limbic encephalitis (Hadjivassiliou et al., 2017; Fredriksen et al., 2018; Ernst et al., 2019; Mitoma et al., 2018). However, these studies were conducted by combining antibodies other than anti-GAD (Hadjivassiliou et al., 2017; Fredriksen et al., 2018; Ernst et al., 2019; Mitoma et al., 2018), and the role of each particular antibody in volumetry is not well understood.

2. Objectives

The objective of this study is to perform quantitative volumetric brain MRI in patients harboring anti-GAD related neurological syndromes. The aim is to highlight possible radiological particularities in our patients compared to a matched healthy cohort, as well as the potential differences in the radiological profile between each clinical phenotype.

3. Materials and methods

3.1. Recruitment and processing

We collected clinical and radiological data retrospectively from patients with neurological disorders associated with anti-GAD antibodies at the Pitié Salpêtrière Hospital in Paris between 2007 and March 2020. The inclusion criteria were: (1) positive anti-GAD antibodies in the blood and/or cerebrospinal fluid (CSF) (2), a clinical presentation compatible with a neurological syndrome associated with anti-GAD antibodies (SPS, CAt or LE) and (3), at least one brain MRI available. Among the 46 patients with positive anti-GAD antibodies identified at the Pitié Salpêtrière laboratory, 20 patients did not have brain MRI available, and were excluded. Finally, 26 patients were included in this study.

3.2. Data availability

Anonymized data that are not published in this article will be available on request from any qualified investigator.

3.3. Selection of control data

For control subjects, we used healthy subjects MRI (without neurological diseases) from two public databases, IXI with 15 patients (Serag et al., 2012) (https://brain-development.org/ixi-dataset/) and Open Access Series of Imaging Studies with 11 patients, OASIS (LaMontagne et al., 2019) (https://www.oasis-brains.org/#datam), matched by sex and age.

3.4. Antibodies testing

Immunological analyses for the diagnosis of anti-GAD antibodies in the blood or CSF were carried out in the laboratory of the Pitié-Salpêtrière hospital by an indirect immunohistochemistry method, as previously described (Pittock et al., 2006). Additional immunoblot analyses were performed to confirm all the immunohistochemistry results. Finally, all the positive results were independently externally validated by the laboratory of Professor Honnorat in Lyon using the same techniques.

3.5. Immunomodulatory treatments

The patients were treated with immunotherapy during their medical care according to expert advice and the recommendations of the scientific societies. Patients could receive intravenous corticosteroids, IV immunoglobulins or plasma exchanges. As second-line treatment, immunosuppressive treatments such as azathioprine, rituximab, cyclophosphamide or mycophenolate mofetil were used.

3.6. Images acquisition

The majority of images were acquired on a 3Tesla MRI (20 out of 26), the remainder on 1.5 T MRI machines (PREMIER, General Electric Healthcare). The median image acquisition criteria were: Repetition Time = 9.6, Echo Time = 4.6, Number of Phase Encoding Steps = 208, Echo Train Length = 208, Reconstruction Diameter = 240, Acquisition Matrix = 208 × 208, Flip Angle = 8.0 with sequence voxels size 1 × 1 mm and slice thickness 1 mm for T1-weighted and voxel size of 1 × 1 mm and slice thickness 2 mm for T2 FLAIR-weighted images.

3.7. Images analysis

The T1 and T2 FLAIR-weighted images were used for the analyses. These sequence imaging from patients and controls were transformed into Neuroimaging Informatics Technology Initiative (NIfTI) format and then subjected to image normalization by N4 Bias Field Correction, to correct errors associated with the non-homogeneity due to the magnetic field, using the n4BiasFieldCorrect function of the package Advanced Normalization Tools in R (ANTsR) (v.0.5.6.1) (Tustison et al., 2010). Afterwards, we used the WhiteStripe R package (v.2.3.2) to normalize the intensities of MRI (on both T1 and T2 FLAIR-weighted images) across the different individuals in this study (Shinohara et al., 2014). Finally, the brain MRIs (T1 and T2 FLAIR-weighted images) from this cohort were co-registered to a reference MRI (Montreal Neurological Institute, MNI152) using an Affine with deformable transformation using the symetric normalization (SyN) (antsRegistration of the ANTsR package).

The automated volumetric analyses for the brain were carried out from the NIfTI T1 files, via the following softwares: Volbrain 1.0, which allows to obtain an automatic volumetric segmentation of the brain (Manjón and Coupé, 2016), CEREbellum Segmentation (CERES) 1.0, which obtains a volumetric segmentation of the different lobules of the cerebellum (Romero et al., 2017a) and the software HIPpocampus subfield Segmentation 1.0 (HIPS), with T1 and T2-weighted sequences (Romero et al., 2017b).

Cortical thickness analysis was performed using FreeSurfer software using the *recon-all* function, version 7.1 for our cohort patients and controls (Fischl, 2012). This analysis includes a tessellation that leads to a 3D mesh of the cortical surface formed by thousands of vertices per hemisphere (~160.000 in total) and we used the fsaverage template. FreeSurfer was used to produce *vertex-wise* maps (Fischl and Dale, 2000). The cortical surfaces of each subject were calibrated to a template and smoothed using a *full-width-at-half maximum* (FWHM) of 10 mm. We used a linear model for each vertex i to compare cortical thickness between groups (anti-GAD and healthy subjects), using age as a continuous covariate, and including residual error : $yi = β0 + β1Group + β3Age + εi$. We used a cluster-level analysis with a cluster formation threshold p = 0.01. We represented clusters with cluster-wise p-value (cwp) of cwp < 0.05. These p-values were corrected for multiple comparisons using the mri_glmfit-sim precomputed MonteCarlo simulation.

Several post-processing steps were followed to limit the bias of multiple acquisition sites. We used the Combat technique to harmonize the data from our acquisition centers, on both T1 and T2 FLAIR-weighted images. This method adjusts the mean value and variance of measurements of characteristics between sites (Fortin et al., 2018).

The radiomic features (n = 62) were obtained with LifeX using the

whole brain of sequences T1 and T2 FLAIR-weighted of our subjects (Nioche et al., 2018). The extracted radiomic features include information regarding the intensity distribution, spatial relationships between different intensity levels, texture heterogeneity patterns, description of the shape and relationships of the lesion with surrounding tissue. The description of the radiomic variables obtained from LifeX is detailed at https://lifexsoft.org/index.php/resources/19-texture/radiomic-features?filter_tag[0]=

4. Statistics

The volumetric analyses (in particular cerebellum and hippocampus), from results obtained by CERES, FreeSurfer and HIPS, were compared to the control cohort with boxplots. The comparisons between the two groups of the different volumetric features were made using a non-parametric Wilcoxon test. The cortical thickness of the cerebellum was obtained by creating an R-function that averages all the thicknesses in each group of individuals combining the thickness data from CERES. We used the same aforementioned model with FreeSurfer for the vertex-wise analysis with CERES data.

The p-values were adjusted for multiple comparisons, using the false discovery rate (FDR) and values inferior than 0.05 were considered as statistically significant [40]. The t-value obtained by the regressions models provided a way to summarize the direction of association (positive or negative) by using the p-value thresholds described previously. We used the fsbrain (v.0.3.0) and ggseg (v.1.5.4) packages in R to represent the results.

The radiomic variables were normalized with a z-score, which expresses the deviation from the mean value. Using R software (v4.0.2) and ComplexHeatmap package (v.2.4.2), we produced a heatmap with an unsupervised hierarchical clustering of radiomic features (T1-weighted and T2 FLAIR-weighted), using Ward clustering and Euclidean distance. The optimal number of clusters was assessed using different approaches: K-means, Partitioning around medioids (PAM), clara and fanny R functions. We performed a random forest model using the caret package (v.6.0–86) with the radiomic data of patients and controls with default parameters without any feature selection. The model was first trained with 80% of the sample (n = 42), using 10 cross-validations. The model was validated with the remaining 20% of the data. The capacity to classify either anti-GAD or healthy subjects was assessed with area under the curve (AUC) statistic.

5. Results

5.1. Clinical description

The anti-GAD cohort antibodies included 26 patients, 77% of whom were women, with a median age at diagnosis of 39 years. Age at diagnosis varied depending on the clinical presentation: patients with LE were younger, with a median age of 34 years, compared with a median of 50 years in patients with SPS and a median of 52 years in patients with CAt phenotype. The main clinical characteristics are presented in Table 1.

The period between the onset of the first symptoms and the achievement of the first brain MRI was highly variable within the cohort, with a median of two years (interquartile range between 3 months and 5 years). Ten patients had a brain MRI within 12 months of the first symptoms; most of them were patients with limbic encephalitis.

Six patients had a SPS presentation, but only two were isolated, the other ones were associated with other clinical phenotypes. Ten patients had a cerebellar syndrome (40% of them were mixed or associated with other symptoms) and ten patients had an initial presentation of LE (10% of them were mixed), complicated for most cases of drug-resistant TLE.

Overall, 6 patients presented a mixed clinical presentation of neurological syndromes associated with anti-GAD (LE/CAt/SPS). Furthermore, among the 16 patients (61.5%) with epileptic seizures in

Table 1
Clinical and demographic data from anti-GAD patients included in this study.

Clinical and demographic data from anti-GAD patients (n = 26)	
Variable name	Value
Age at diagnosis (years): median [Q1-Q3]	39 [30–52]
Female (%)	20/26 (76.9)
Number of patients with GAD65 Ab positive in blood (%)	25/26 (96.1)
Number of patients with GAD65 Ab positive in CSF (%)	22/26 (84.6)
Time between the first symptom and the first MRI (years): median [Q1-Q3]	2 [0.4–5]
Autoimmune thyroiditis (%)	3/26 (11.6)
Type 1 diabetes (%)	2/26 (7.7)
Malignant tumor (%)	2/26 (7.7)
SPS (%)	6/26 (23)
Cerebellar ataxia (%)	10/26 (38.5)
Limbic encephalitis (%)	10/26 (38.5)
Temporal lobe epilepsy (%)	6/26 (23)
Mixed presentation (%)	6/26 (23)

Q, quartile; CSF, cerebrospinal fluid; GAD, glutamic acid decarboxylase; SPS, stiff-man syndrome.

our cohort, 50% had drug-resistant epilepsy.

Preliminary radiological description was normal in 10 patients (38.5%) of MRIs of our patients, in 10 additional patients (38.5%) MRIs showed hippocampal abnormalities (FLAIR-weighted hyperintensities or atrophy, unilaterally or bilaterally) and cerebellar atrophy was found in 3 patients (11.5%).

5.2. Hippocampal volumetric analysis

The HIPS approach allowed us to obtain the hippocampus subfield (including, the cornus ammonis (CA)1, CA2/CA3, CA4/dentate gyrus, the stratum radiatum/stratum lacunosum/stratum moleculare, the subiculum and the overall hippocampus volume) using standard morphological MRI (Romero et al., 2017b). These volumetric pairwise comparisons of hippocampus structures by subfield from anti-GAD patients versus healthy subject did not pinpoint any significant difference between the whole cohort of anti-GAD patients or when using only a subset of the cohort with LE phenotype versus the control group after adjusting for multiple test comparison (Supplemental Data – Fig. 1). It should be noted that there was a non-significant atrophy of the total hippocampus volume when comparing anti-GAD patients versus control subjects (median volume of 4.3 mm3 vs 5 mm3, respectively, FDR p-value = 0.1).

5.3. Cerebellar volumetric and vertex-wise analysis

Overall, cerebellar vertex-wise analysis showed similar values in anti-GAD patients versus healthy individuals (Fig. 1 A-D). However, some particular cerebellar regions were significantly atrophied in anti-GAD patients (highlighted in blue). We found a significant focal atrophy of the cerebellar cortex, in particular of the left and right V-lobules (Fig. 1D and Supplemental Data – Fig. 2). Conversely, surprisingly, several cerebellar regions were thicker, in anti-GAD when compared to healthy subjects, including the mean thickness of II lobule and left VIIB lobule. The complete list of normalized pairwise comparison of the different cerebellar lobules between anti-GAD patients versus healthy subjects is presented in the Supplemental Data – Fig. 2.

5.4. Unsupervised hierarchical clustering of the radiomic data

Radiomics features included first-order statistics (i.e. mean, median, kurtosis, standard deviation, etc), shape and histogram derived values
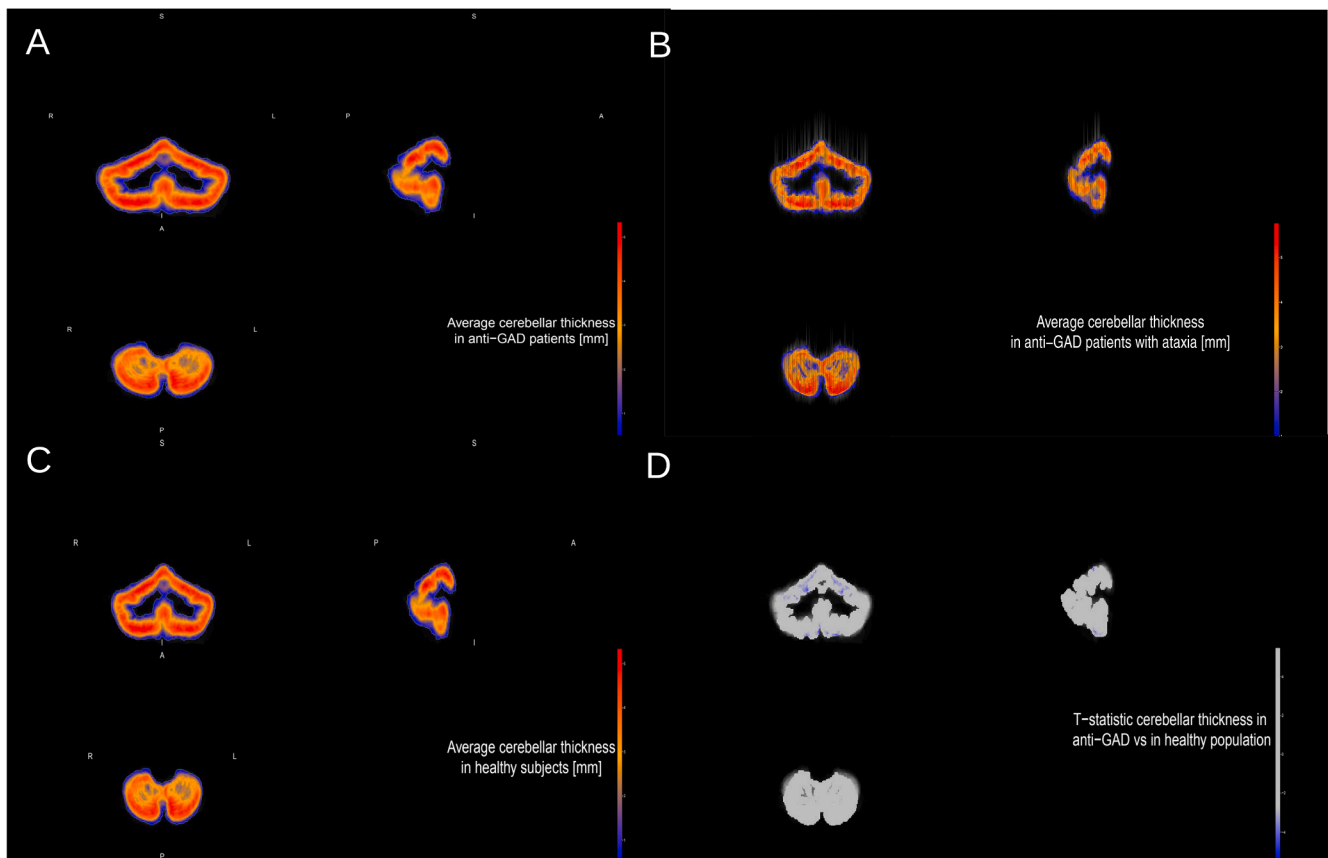
Fig. 1. Representation of cerebellar cortical thickness of the anti-GAD cohort of all phenotypes (A), cerebellar ataxia phenotype only (B), and healthy subjects (C). Comparative analyses of using a voxel-wise approach comparing the cerebellar thickness of anti-GAD patients versus healthy subjects showing the significant atrophy regions in blue represent the t-statistic value with $p < 0.05$, adjusted for multiple comparisons (D). S, superior; I, inferior; A, anterior; P, posterior; R, right; L, left. (For interpretation of the references to colour in this figure legend, the reader is referred to the web version of this article.)

and texture features based on matrix computation of the quantization of gray-levels of the analyzed images. We represented the z-score from the 62 radiomic features using an unsupervised hierarchical clustering (T1 and FLAIR-weighted images). This analysis splitted the anti-GAD patients into two different clusters (Fig. 2). Importantly, the optimal number of clusters using the radiomics features was two using different approaches (Supplemental Data – Fig. 3). Interestingly, the SPS phenotype was only found in the cluster 2 (Fig. 2A). On the contrary, the cluster 1 was enriched with LE phenotype and it included mostly younger patients with a median age in cluster 1 of 22.5 years versus 41 years in the cluster 2, $p = 0.01$ (Fig. 2A). In the same light, the cluster 1 was enriched with higher values from first-order and shape features (Fig. 2A).

5.5. Random forest classification

We also analyzed the classification ability of the radiomic variables to identify the anti-GAD phenotype. After training a random forest model, we could robustly classify anti-GAD MRIs with an AUC = 0.978, (Fig. 2B) with a sensitivity of 100%, specificity of 80% and an accuracy of 90%.

5.6. Cortical thickness and vertex-wise analysis

The average cortical thickness from the results obtained by Free-Surfer in the anti-GAD and the healthy cohorts is presented in Fig. 3A and 3B, respectively. Vertex-wise regression results adjusted by age, highlighted a significant selective loss of the cortical thickness in the temporal lobe bilaterally (particularly in the temporal pole) and in the

frontal lobe in superior, Fig. 4A. Conversely, we found a discrete increase in the thickness at the orbito-frontal lobe, after adjustment for multiple tests, FDR < 0.05, Fig. 4A. Interestingly, the same model after removing anti-GAD with LE, found the same regions but with larger boundaries due to smaller size, Fig. 4B. The cortical thickness data obtained with FreeSurfer was also represented by region or lobes to compare the values of anti-GAD cohort versus the control group, Supplemental Data – Fig. 4 and Supplemental Data – Fig. 5. There was a significant difference with a selective cortical atrophy in the entorhinal region and the temporal pole bilaterally, as well as in the left superior-frontal region and in the region of the right isthmus-cingulate, Fig. 4A and Supplemental Data – Fig. 4 and Supplemental Data – Fig. 5. Intriguingly, the cortical thickness was increased in the *peri*-calcarine region bilaterally and in the lingual left region, Fig. 4A and Supplemental Data - Fig. 4 and Supplemental data – Fig. 5.

6. Discussion

We performed a volumetric and radiomic analysis of brain MRIs of patients with neurological syndromes associated with anti-GAD antibodies, compared to matched by age and sex healthy cohort.

There is little detailed data on brain imagery of anti-GAD patients in the literature, showing often normal findings in the initial phase or some minor abnormalities (Meinck and Thompson, 2002; Ernst et al., 2019). The scarce available studies with volumetric analysis of limbic structures that have concerned only anti-GAD patients with LE phenotype (Wagner et al., 2015; Ernst et al., 2019). These studies did not find a focal hippocampal atrophy but an increased volume of the CA1 region of the hippocampus for the first study and an increased volume of the
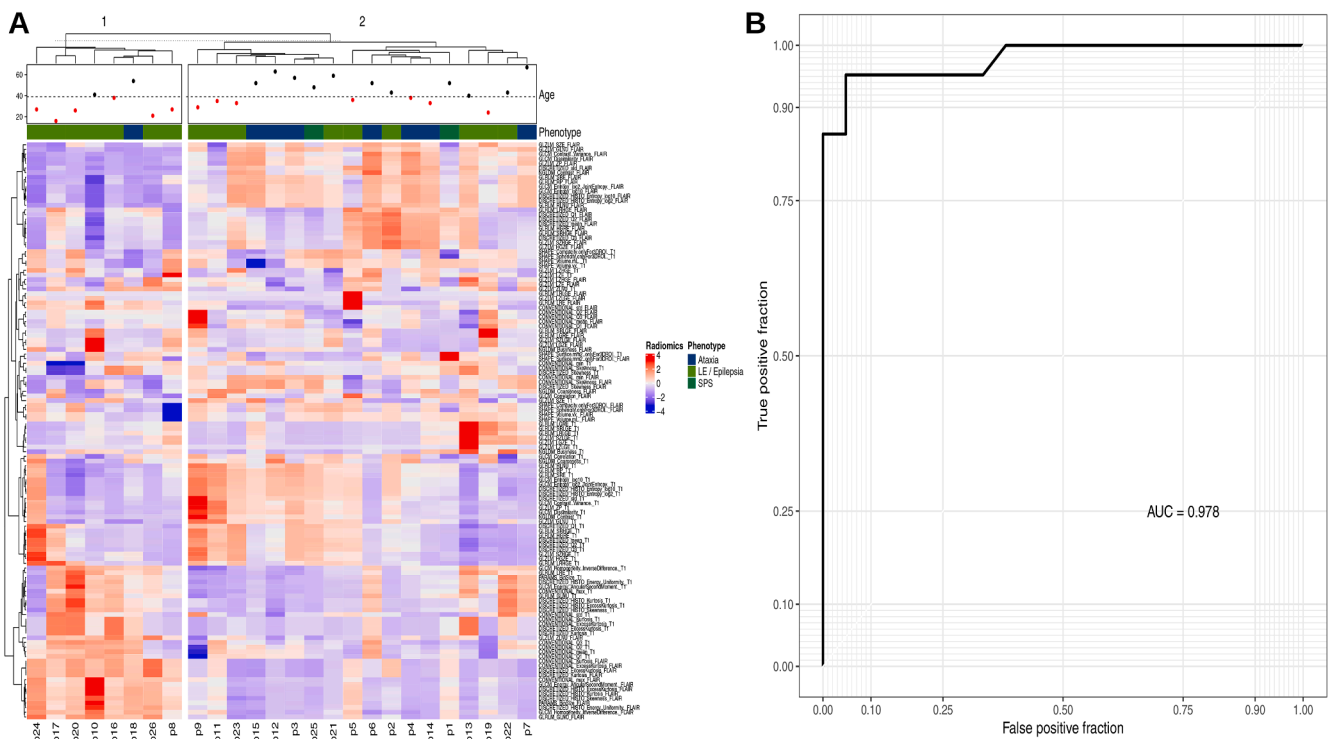
Fig. 2. A) Heatmap of the 62 radiomic variables extracted from the T1 and T2 FLAIR-weighted imaging of the 26 patients with neurological syndromes associated with anti-GAD antibodies. The heatmap shows the values of the radiomic variables expressed in Z-scores, the left column details the different radiomic features. The age (depicted in red if age is below the median of 39-year or black if it is above this cut-off) and the anti-GAD phenotype are indicated in the legend. B) Receiver operating characteristic (ROC) curve for predictive value of radiomic variables to classify MRI as "anti-GAD" (For interpretation of the references to colour in this figure legend, the reader is referred to the web version of this article.)
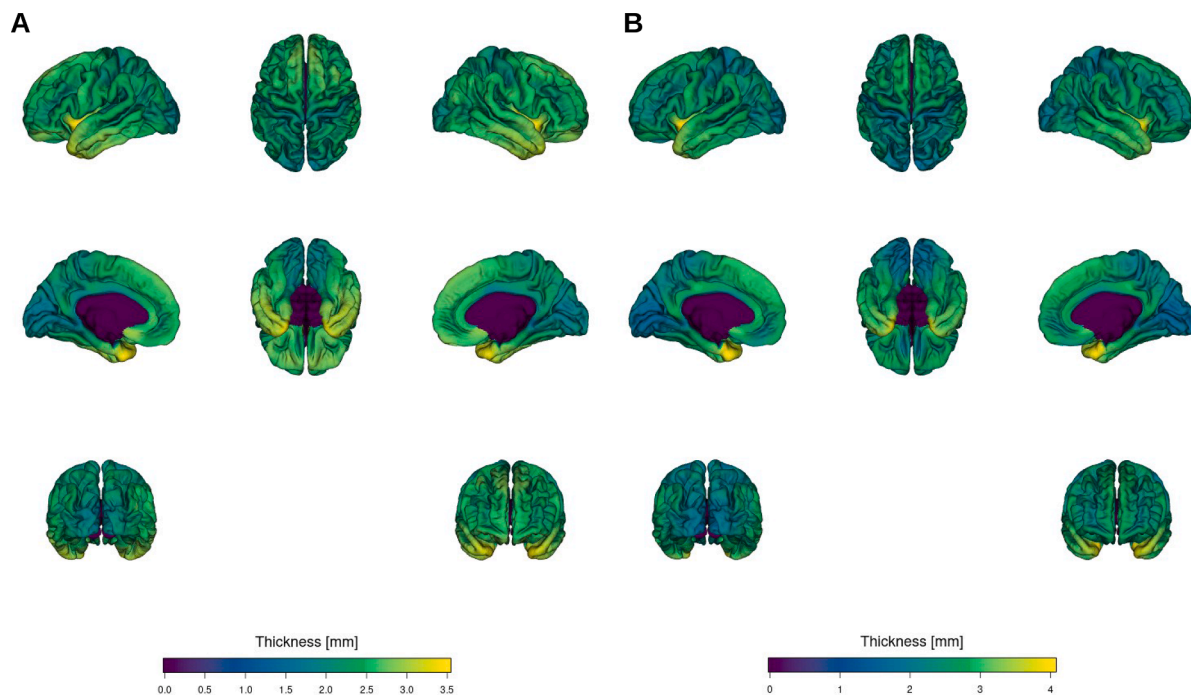

Fig. 3. The average cortical thickness obtained from FreeSurfer in all anti-GAD patients included in this study (A) and in the healthy subjects (B).

amygdala for the other. Likewise, we did not find any significant difference in the volumetric subfield data at hippocampal level, but a slight atrophy in the mean hippocampal volume (FDR p-value = 0.1), suggesting that we lacked power to detect these differences.

The results of our study suggest that, regardless of the phenotype, there are abnormalities of cortical thickness in several regions of the brain, including a selective atrophy in the temporal lobe (entorhinal cortex, temporal pole) and frontal lobes. Interestingly, several studies
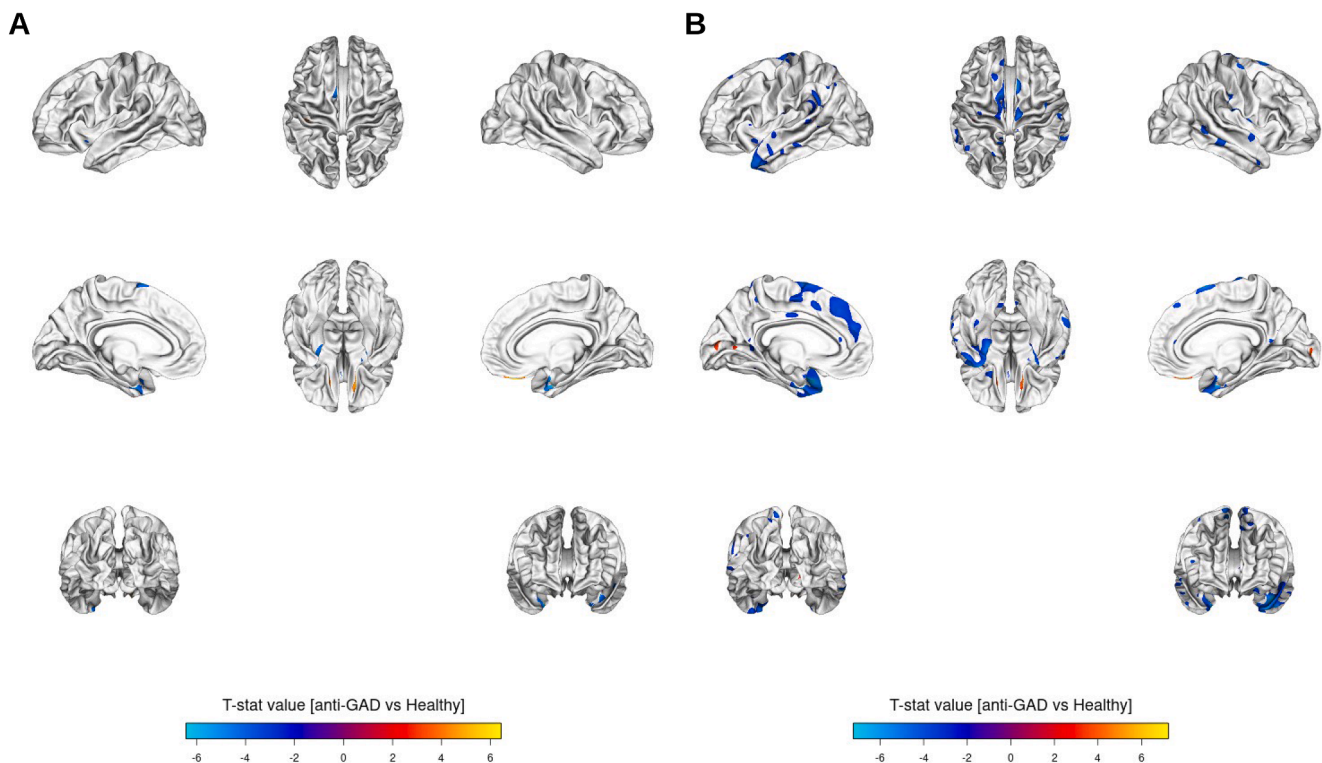
A   **B**

T-stat value [anti-GAD vs Healthy]

-6   -4   -2   0   2   4   6

T-stat value [anti-GAD vs Healthy]

-6   -4   -2   0   2   4   6

Fig. 4. Comparative tests of the cortical thickness of patients compared to healthy subjects (a) all patients and (b) all patients except those with limbic encephalitis (FreeSurfer data).

have highlighted the role of the entorhinal cortex in the electro-genesis of temporal lobe epilepsies (Parrent and Blume, 1999; Bernasconi et al., 2001; Noulhiane et al., 2006). The entorhinal cortex is interconnected with many cortical and subcortical regions, but also with the hippocampus within the mesial temporal region (Kerr et al., 2007). The entorhinal cortex could therefore be an affected region, playing a key pathophysiological role in autoimmune anti-GAD involvement, especially in LE phenotypes. Furthermore, regarding the increase in the cortical thickness of the orbito-frontal region, it is tempting to speculate that there would be a compensatory effect in this region, related with a recruitment of additional cortical regions, following a cerebral atrophy, particularly the temporal atrophy. Indeed, this compensatory mechanism of relocation of cognitive resources has already been demonstrated in patients with Alzheimer's disease, with an overactivity of the prefrontal cortex (Grady et al., 2003). There are strong associations between the fronto-orbital cortex and the limbic and paralimbic regions (in particular the entorhinal cortex) (Stoodley et al., 2012) which could explain this phenomenon. Another hypothesis would be a specific encephalitic impairment of this region causing local inflammation and a local increase in volume. In the same light, we found a focal atrophy in the motor cerebellar V-lobule and a higher cortical thickness in several non-motor cerebellar areas (i.e. II and VIIB lobules). Our results also suggest that this atrophy is found across all phenotypes. The V-lobule is a motor lobule activated during motor tasks involving fingers movements. In addition, several connectivity studies have shown that the activity of the sensory-motor cortex is correlated with the activity of the cerebellar lobules V, VI and VIII (Buckner et al., 2011), with a somatic motor representation in the anterior lobe of the cerebellum (D'Mello et al., 2015). This connectivity study also suggests connections of the anterior cerebellum with the associative cortex and the limbic system, highlighting the crosstalk between these two networks (D'Mello et al., 2015). Interestingly, a variety of non-motor cerebellar lobules (i.e. lobule II and VIIB) had a higher cortical thickness. Similar results have been pinpointed in patients with TLE (Marcián et al., 2018). Therefore, future

functional MRI and connectivity studies should deepen the potential role of cerebellum in long-term cognition in these patients.

Radiomics refers to the high-throughput extraction of large amounts of quantitative features of medical images (Lambin et al., 2012). This approach has been mainly used in cancer imaging but it could be implemented in other areas. The radiomic analysis using a random forest model allowed us to correctly classify the MRI from anti-GAD when compared to the MRI of the control group. These results should be interpreted with caution because of the small sample size, the whole brain extraction and the acquisition technique differences of our MRI. Indeed, we extracted the radiomic data from the whole brain, unlike the majority of studies which only extract the lesion area. It should be noted that the signal abnormalities in our patients were limited to a few hyperintensities of limbic structures in certain cases of limbic encephalitis or hyperintensities of white matter and not related to anti-GAD antibodies and in the vast majority of cases the MRI could be considered as normal. Therefore, we decided to use the entire brain in order to have exhaustive data to compare the three phenotypes. Future studies should assess the performance to classify anti-GAD MRI when compared to other neurological diseases, with more standardized acquisition protocols between patients and controls. Another shortcoming of the radiomics features is related to their direct interpretation. It is difficult to interpret a particular radiomic feature individually. In our study, the cluster 1 of unsupervised hierarchical clustering from radiomics was enriched with first-order statistics features, suggesting that the MRIs of the patients belonging to this cluster were more homogenous.

It is worth noting that our study has several limitations. It is a retrospective analysis of the clinical and radiological data of patients from a single institution. The neurological disorders associated with anti-GAD autoimmunity are rare, which explains the low number of patients included. In addition, the MRI of our patients (due to the retrospective nature and their limited number) were acquired according to heterogeneous protocols, on different machines (1.5 T, 3 T),. However, we applied different pre-process and post-process steps to limit the

impact of these potential drawbacks.

This study provides a comprehensive radiological description of the autoimmune neurological pathology associated with anti-GAD antibodies, using advanced MRI analyses. The radiological peculiarities of the patients in our cohort, by identifying the precise structures affected, can provide a better understanding of the pathophysiology, which is still partially unknown. Moreover, if the specific anti-GAD nature of these radiological abnormalities is confirmed after additional analyzes in other etiologies of encephalitis, these advanced MRI analysis techniques could be a complementary diagnostic tool in this type of impairment in the near future.

7. Conclusion

This study highlighted a particular radiological profile in our subjects with neurological syndrome associated with anti-GAD antibodies, all phenotypes combined. Our results suggest that anti-GAD phenotypes should be considered as a continuum because of the similar atrophy patterns found, independently of the anti-GAD phenotype. Future functional and connectivity imaging analysis in neurological autoimmune diseases are warranted, in order to strengthen the brain and cerebellar networks involved in autoimmune encephalitis.

CRediT authorship contribution statement

Maëlle Dade: Data curation. **Marine Giry:** Data curation. **Giulia Berzero:** Data curation, Writing - review & editing. **Marion Benazra:** Data curation. **Gilles Huberfeld:** Data curation, Writing - review & editing. **Delphine Leclercq:** Writing - review & editing. **Vincent Navarro:** Writing - review & editing. **Jean-Yves Delattre:** Writing - review & editing. **Dimitri Psimaras:** Data curation, Writing - review & editing. **Agusti Alentorn:** Data curation, Supervision, Methodology.

Declaration of Competing Interest

The authors declare that they have no known competing financial interests or personal relationships that could have appeared to influence the work reported in this paper.

Appendix A. Supplementary data

Supplementary data to this article can be found online at https://doi.org/10.1016/j.nicl.2021.102826.

References

Bernasconi, N., Bernasconi, A., Caramanos, Z., Dubeau, F., Richardson, J., Andermann, F., Arnold, D.L., 2001. Entorhinal cortex atrophy in epilepsy patients exhibiting normal hippocampal volumes. Neurology 56 (10), 1335–1339.

Buckner, R.L., Krienen, F.M., Castellanos, A., Diaz, J.C., Yeo, B.T.T., 2011. The organization of the human cerebellum estimated by intrinsic functional connectivity. J. Neurophysiol. 106 (5), 2322–2345.

D'Mello, A.M., Crocetti, D., Mostofsky, S.H., Stoodley, C.J., 2015. Cerebellar gray matter and lobular volumes correlate with core autism symptoms. Neuroimage Clin. 7, 631–639.

Ernst, L., David, B., Gaubatz, J., Domínguez-Narciso, I., Lüchters, G., Becker, A.J., et al. Volumetry of Mesiotemporal Structures Reflects Serostatus in Patients with Limbic Encephalitis. AJNR Am. J. Neuroradiol. 2019; 40: 2081–9.

Fischl, B., FreeSurfer. Neuroimage 2012; 62: 774–81.

Fischl, B., Dale, A.M., 2000. Measuring the thickness of the human cerebral cortex from magnetic resonance images. Proc Natl Acad Sci U S A 97 (20), 11050–11055.

Fortin, J.-P., Cullen, N., Sheline, Y.I., Taylor, W.D., Aselcioglu, I., Cook, P.A., Adams, P., Cooper, C., Fava, M., McGrath, P.J., McInnis, M., Phillips, M.L., Trivedi, M.H., Weissman, M.M., Shinohara, R.T., 2018. Harmonization of cortical thickness measurements across scanners and sites. Neuroimage 167, 104–120.

Fredriksen, J.R., Carr, C.M., Koeller, K.K., Verdoorn, J.T., Gadoth, A., Pittock, S.J., Kotsenas, A.L., 2018. MRI findings in glutamic acid decarboxylase associated autoimmune epilepsy. Neuroradiology 60 (3), 239–245.

Grady, C.L., McIntosh, A.R., Beig, S., Keightley, M.L., Burian, H., Black, S.E., 2003. Evidence from functional neuroimaging of a compensatory prefrontal network in Alzheimer's disease. J. Neurosci 23 (3), 986–993.

Graus, F., Saiz, A., Dalmau, J., 2010. Antibodies and neuronal autoimmune disorders of the CNS. J. Neurol. 257 (4), 509–517.

Graus, F., Saiz, A., Dalmau, J., 2020. GAD antibodies in neurological disorders - insights and challenges. Nat. Rev.Neurol 16 (7), 353–365.

Hadjivassiliou, M., Martindale, J., Shanmugarajah, P., Grünewald, R.A., Sarrigiannis, P. G., Beauchamp, N., Garrard, K., Warburton, R., Sanders, D.S., Friend, D., Duty, S., Taylor, J., Hoggard, N., 2017. Causes of progressive cerebellar ataxia: prospective evaluation of 1500 patients. J Neurol Neurosurg. Psychiatry 88 (4), 301–309.

Hansen, N., Grünewald, B., Weishaupt, A., Colaço, M.N., Toyka, K.V., Sommer, C., Geis, C., 2013. Human Stiff person syndrome IgG-containing high-titer anti-GAD65 autoantibodies induce motor dysfunction in rats. Exp. Neurol. 239, 202–209.

Jin, H., Wu, H., Osterhaus, G., Wei, J., Davis, K., Sha, D., et al. 2003. Demonstration of functional coupling between gamma -aminobutyric acid (GABA) synthesis and vesicular GABA transport into synaptic vesicles. Proc. Natl. Acad. Sci. U. S. A. 100, 4293–4298.

Kerr, K.M., Agster, K.L., Furtak, S.C., Burwell, R.D., 2007. Functional neuroanatomy of the parahippocampal region: the lateral and medial entorhinal areas. Hippocampus 17 (9), 697–708.

Koerner, C., Wieland, B., Richter, W., Meinck, H.-M., 2004. Stiff-person syndromes: motor cortex hyperexcitability correlates with anti-GAD autoimmunity. Neurology 62 (8), 1357–1362.

Lambin, P., Rios-Velazquez, E., Leijenaar, R., Carvalho, S., van Stiphout, R.G.P.M., Granton, P., Zegers, C.M.L., Gillies, R., Boellard, R., Dekker, A., Aerts, H.J.W.L., 2012. Radiomics: extracting more information from medical images using advanced feature analysis. Eur. J. Cancer. 48 (4), 441–446.

LaMontagne, P.J., Benzinger, T.L., Morri, J.C., Keefe, S., Hornbeck, R., Xiong C, et al. OASIS-3: Longitudinal Neuroimaging, Clinical, and Cognitive Dataset for Normal Aging and Alzheimer Disease. medRxiv 2019: 2019.12.13.19014902.

Malter, M.P., Helmstaedter, C., Urbach, H., Vincent, A., Bien, C.G., 2010. Antibodies to glutamic acid decarboxylase define a form of limbic encephalitis. Ann. Neurol. 67 (4), 470–478.

Manjón, J.V., Coupé, P., 2016. volBrain: An Online MRI Brain Volumetry System. Front. Neuroinform. 10, 30.

Marcián, V., Mareček, R., Koriťáková, E., Pail, M., Bareš, M., Brázdil, M., 2018. Morphological changes of cerebellar substructures in temporal lobe epilepsy: A complex phenomenon, not mere atrophy. Seizure 54, 51–57.

McKeon, A., Tracy, J.A., 2017. GAD65 neurological autoimmunity. Muscle Nerve 56 (1), 15–27.

Meinck, H.-M., Thompson, P.D., 2002. Stiff man syndrome and related conditions. Mov Disord 17 (5), 853–866.

Mitoma, H., Manto, M., Hampe, C.S., 2018. Immune-mediated cerebellar ataxias: practical guidelines and therapeutic challenges. Curr. Neuropharmacol. 17 (1), 33–58.

Nioche, C., Orlhac, F., Boughdad, S., Reuzé, S., Goya-Outi, J., Robert, C., Pellot-Barakat, C., Soussan, M., Frouin, F., Buvat, I., 2018. LIFEx: A Freeware for Radiomic Feature Calculation in Multimodality Imaging to Accelerate Advances in the Characterization of Tumor Heterogeneity. Cancer Res. 78 (16), 4786–4789.

Noulhiane, M., Samson, S., Clémenceau, S., Dormont, D., Baulac, M., Hasboun, D., 2006. A volumetric MRI study of the hippocampus and the parahippocampal region after unilateral medial temporal lobe resection. J. Neurosci. Methods 156 (1-2), 293–304.

Parrent, A.G., Blume, W.T., 1999. Stereotactic amygdalohippocampotomy for the treatment of medial temporal lobe epilepsy. Epilepsia 40 (11), 1408–1416.

Paschou, S.A., Papadopoulou-Marketou, N., Chrousos, G.P., Kanaka-Gentenbein. C., On type 1 diabetes mellitus pathogenesis. Endocr Connect 2018; 7: R38–46.

Pittock, S.J., Yoshikawa, H., Ahlskog, J.E., Tisch, S.H., Benarroch, E.E., Kryzer, T.J., Lennon, V.A., 2006. Glutamic acid decarboxylase autoimmunity with brainstem, extrapyramidal, and spinal cord dysfunction. Mayo Clin. Proc. 81 (9), 1207–1214.

Romero, J.E., Coupé, P., Giraud, R., Ta, V.-T., Fonov, V., Park, M.T.M., Chakravarty, M. M., Voineskos, A.N., Manjón, J.V., 2017a. CERES: A new cerebellum lobule segmentation method. Neuroimage 147, 916–924.

Romero, J.E., Coupé, P., Manjón, J.V., 2017b. HIPS: A new hippocampus subfield segmentation method. Neuroimage 163, 286–295.

Saiz A, Blanco Y, Sabater L, González F, Bataller L, Casamitjana R, et al. Spectrum of neurological syndromes associated with glutamic acid decarboxylase antibodies: diagnostic clues for this association. Brain 2008; 131: 2553–63.

Serag, A., Aljabar, P., Ball, G., Counsell, S.J., Boardman, J.P., Rutherford, M.A., Edwards, A.D., Hajnal, J.V., Rueckert, D., 2012. Construction of a consistent high-definition spatio-temporal atlas of the developing brain using adaptive kernel regression. Neuroimage 59 (3), 2255–2265.

Shinohara, R.T., Sweeney, E.M., Goldsmith, J., Shiee, N., Mateen, F.J., Calabresi, P.A., Jarso, S., Pham, D.L., Reich, D.S., Crainiceanu, C.M., 2014. Statistical normalization techniques for magnetic resonance imaging. Neuroimage Clin. 6, 9–19.

Solimena, M., De Camilli, P., 1991. Autoimmunity to glutamic acid decarboxylase (GAD) in Stiff-Man syndrome and insulin-dependent diabetes mellitus. Trends Neurosci. 14 (10), 452–457.

Stoodley, C.J., Valera, E.M., Schmahmann, J.D., 2012. Functional topography of the cerebellum for motor and cognitive tasks: an fMRI study. Neuroimage 59 (2), 1560–1570.

Tian, N., Petersen, C., Kash, S., Baekkeskov, S., Copenhagen, D., Nicoll, R., 1999. The role of the synthetic enzyme GAD65 in the control of neuronal gamma-aminobutyric acid release. Proc. Natl. Acad. Sci. U. S. A. 96 (22), 12911–12916.

Tustison, N.J., Avants, B.B., Cook, P.A., Yuanjie Zheng, Egan, A., Yushkevich, P.A., Gee, J.C., 2010. N4ITK: improved N3 bias correction. IEEE Trans. Med. Imaging 29 (6), 1310–1320.

Vincent, S.R., Hökfelt, T., Wu, J.-Y., Elde, R.P., Morgan, L.M., Kimmel, J.R., 1983. Immunohistochemical studies of the GABA system in the pancreas. Neuroendocrinology 36 (3), 197–204.

Wagner, J., Witt, J.-A., Helmstaedter, C., Malter, M.P., Weber, B., Elger, C.E., 2015. Automated volumetry of the mesiotemporal structures in antibody-associated limbic encephalitis. J. Neurol. Neurosurg. Psychiatry 86 (7), 735–742.